S. M. Cheng
Research Officer,
Institute for Aerospace Research,
National Research Council Canada,
Montreal Road, M-7,
Ottawa, ON, Canada K1A 0R6
Assoc. Mem. ASME,
e-mail: shumin.cheng@nrc.ca

A. S. J. Swamidas
Professor,
Faculty of Engineering and Applied Science,
Memorial University of Newfoundland,
St. John's, NF, Canada A1B 3X5
Mem. ASME

W. Wallace
Director.

X. Wu
Research Officer.

Institute for Aerospace Research,
National Research Council Canada,
Montreal Road,
Ottawa, ON, Canada K1A 0R6

An Experimental Investigation of Tubular T-Joints Under Cyclic Loads

This paper presents an experimental study of fatigue crack initiation and growth in tubular T-joints, simulating the extreme case of those used for offshore platforms. The crack locations and profiles were recorded and fractographic examinations were carried out to reveal the mechanisms of crack initiation, growth, and crack closure. The relationships between crack length/depth and the numbers of fatigue cycle were analyzed using the Paris equation. During testing, the static strain responses at selected gage locations were also recorded. The variations in the static strains caused by the formation and growth of cracks were correlated with fatigue cycles by a characteristic equation. These results and correlations are useful for understanding the fatigue damage process and for monitoring the development of such damage in tubular T-joints of offshore structures.

1 Introduction

Tubular T-joints have a long history of use in offshore platforms, bridges, and other civil engineering structures. Even though the design stress (using the load factor approach) in the tubular T-joints is nominally below the yield strength of the material, as required by the design codes, winds, waves, currents, and seasonal storms often introduce cyclic loads which might cause fatigue damage accumulation, apart from corrosion and other forms of environmental degradation.

Fatigue testing of tubular joints to assess their fatigue lives have been carried out globally on a variety of tubular joints (T, Y, K, X, YT, DY, DK, and DT) during the past three decades. These studies have assessed the fatigue strength (relating nominal weld toe stress range to fatigue life), crack initiation, propagation and development, and the nondestructive measurement of crack growth using ACFM/DCPD/ultrasonic techniques (Bouwkamp, 1966; Maeda et al., 1969; Natarajan and Toprac, 1968; Dijkstra and deBack, 1980; Dover and Holdbrook, 1979; Gibstein, 1981; Lida et al., 1981; Leiurada and Gerald, 1981; Wylde, 1983; Gurney, 1989; Lambert et al., 1987; Pederson and Aserskov, 1991; and Recho, 1990). These studies have reported the fatigue behavior of simple and complex tubular joints under cyclic/random fatigue loads; most have examined the crack growth development and prediction in tubular joints under cyclic/random loads, but none have presented fatigue crack growth analysis in detail at the microscopic level. Moreover, all these studies on crack growth measurement and prediction were based on static measurements carried out when the tubular joints under test were at rest. No study has yet been reported on crack measurement and prediction under dynamic testing conditions.

In this study, fatigue tests were conducted on three geometrically similar tubular T-joint specimens to study the process of crack initiation and growth. The results of fatigue response analysis and fractographic analysis are presented in this paper. The mechanical and metallurgical observations are correlated to give a full description of the crack initiation/growth process in tubular T-joints.

2 Experimental Setup and Testing

The geometry of the tubular T-joint specimens was designed to be representative of the joints used for small and medium-sized offshore platforms. The dimensions (in mm) are given in Fig. 1. The specimens were made from CSA G40.21-92 50W CLS. C. ERW steel. The basic mechanical properties of the material are given in Table 1.

During fabrication of the specimens, two tubular members, one serving as the chord and the other as the brace, were joined together initially by spot welding. Welding was completed using the shielded metal arc welding technique in accordance with CSA Standard W59-1982 "Welded Steel Construction" (Metal Arc Welding). A special load frame was constructed to carry out the fatigue test, as shown in Fig. 2. The actuator was mounted on the top of the frame, and was lined up to be truly vertical. The verticality of the brace and the horizontality of the chord were checked with reference to the actuator and the load frame. However, even with our best effort, a slight eccentricity in the brace/chord joining was introduced during welding. This eccentricity resulted in assembly stresses and lead to asymmetrical cracking during the testing, as discussed later. In the testing, a hydraulic actuator (MTS series 244, which was controlled by a controller, MTS 407) was used to apply fatigue loads, at a frequency of 5 Hz, in the axial direction of the brace. The load ranges and load ratios ($R = P_{min}/P_{max}$) applied to the three specimens, as given in Table 2, are representative of fatigue design loads. Modal testing was also conducted at selected crack lengths to study the dynamic response of the specimens in the presence of these weld toe cracks. Details of modal testing are described in a separate paper (Cheng

Contributed by the OMAE Division for publication in the JOURNAL OF OFFSHORE MECHANICS AND ARCTIC ENGINEERING. Manuscript received by the OMAE Division, July 1998; revised manuscript received April 7, 1999. Associate Technical Editor: J. E. Indacochea.

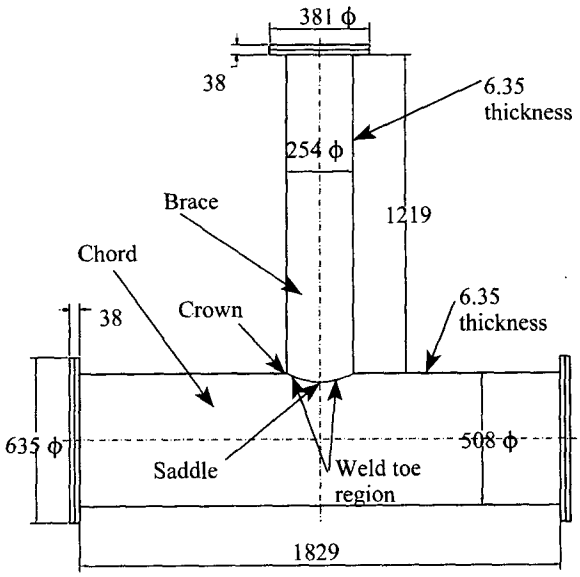

All dimensions in mm

Fig. 1 Tubular T-joint

et al., 1999). This part of the testing may have some influence on fatigue cracks as discussed later.

The load levels were chosen such that the nominal stresses at the saddle points of the weld toe in all specimens were identical, and measured by strain gages to be 250 MPa. Because of the eccentricity introduced by assembly, stress at one side of the saddle point was found to be slightly different from that at the other side. Therefore, most of the cracks occurred on the high-stress side of the weld toe. All equipment used in testing was carefully calibrated to ensure accuracy, and all tests were performed in laboratory air at ambient temperature.

3 Crack Profile Determination

Fatigue crack profiles were recorded by ink staining and beach marking during testing. The inking was performed when the cracks became visible to the naked eye. The existence of the cracks was then confirmed by observing the "pumping in and out" of isopropyl alcohol applied to suspected crack locations. The inking medium was a slow-drying red ink made from fingernail polish diluted with 100 percent pure isopropyl alcohol. This red ink stain stayed permanently and clearly marked the initial crack profile. Beach marking was performed by doubling the cyclic frequency and halving the fatigue load range for 60,000–120,000 cycles. Digitized photographs of the crack profiles were taken for the three specimens after cutting open the cracked section of the weld toe. A typical cracking location and the region cut for fractographic examination are shown schematically in Fig. 3. Figures 4 and 5 show the crack profiles in specimens 2 and 3 for purpose of illustration. It was noticed that in specimens 1 and 3, a single large crack had formed on only one side of the weld toe (side 1, which had experienced a slightly larger stress than the other side due to the loading eccentricity) of the chord, while in specimen 2 by the time of inking, multiple thumbnail cracks had developed on both sides of the chord.

In specimen 2, as shown in Fig. 4, two large thumbnail cracks had almost joined together by the time of inking. A closer look at the right side of the nearly joined cracks revealed three additional small thumbnail cracks that had not yet coalesced. In the present

Table 1 Nominal tensile properties of CSA G40.21-92 50W CLS. C. ERW steel

Ultimate tensile strength (MPa)	Yield (2 percent offset) strength (MPa)	Elongation (percent)
556	405	24

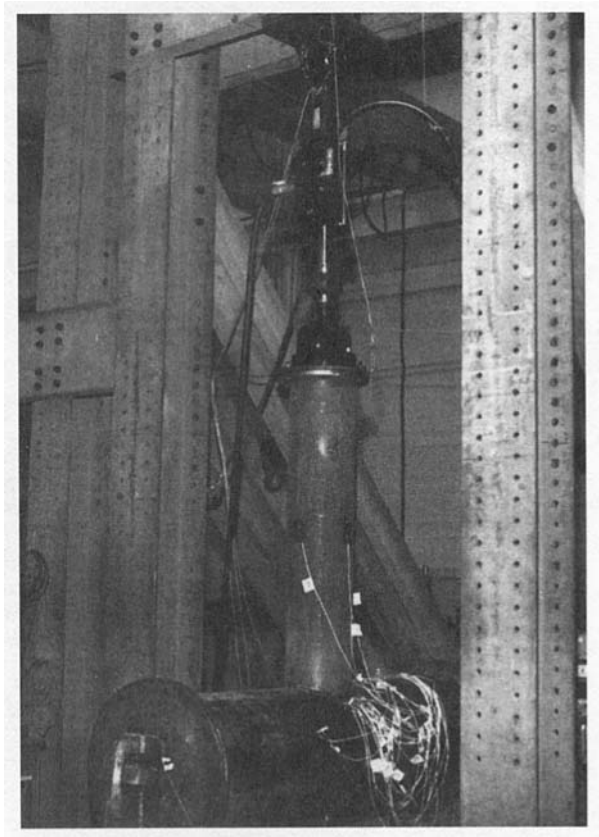

Fig. 2 Fatigue test

Table 2 Fatigue loads

Specimen no.	Load range (N)	Load ratio
1	33109	0.2
2	35603	0.2
3	33630	0

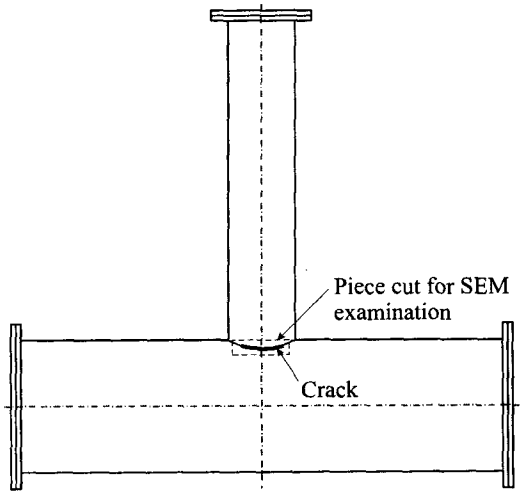

Fig. 3 Coupon cut for SEM examination

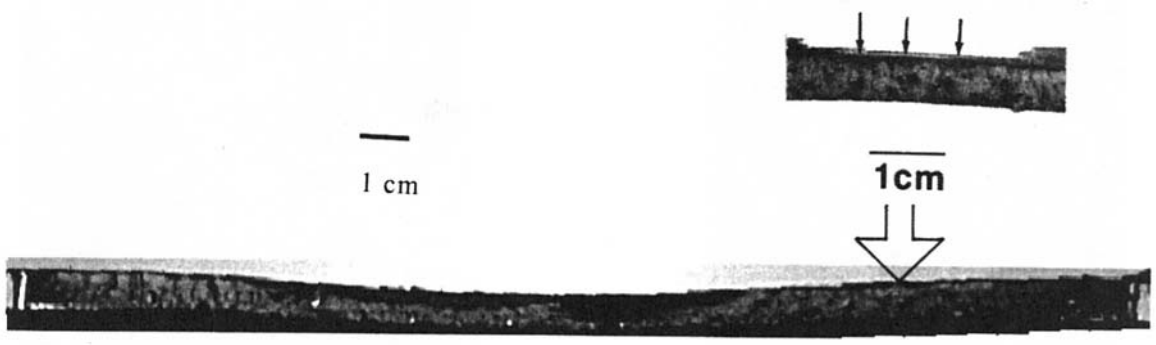

Fig. 4 Photo of crack profile for specimen 2, side 1

study, it was impossible to determine whether the large semi-elliptical cracks in specimens 2 and 3 had started life as individual thumbnail cracks or whether they were formed by successive coalescence of several smaller thumbnail cracks that had occurred earlier. In all specimens, the semi-elliptical cracks would eventually break through the thickness of the chord after a certain number of fatigue cycles and become a large through-the-thickness crack.

4 Fracture Surface Analysis

Fracture surfaces from specimens 2 and 3 were examined using an Hitachi S-570 scanning electron microscope (SEM). The studies, reported in the forthcoming, provided information on the crack initiation process at the early stages of fatigue crack growth.

The optical photographs, Fig. 4, showed that the fatigue fracture process had occurred by the formation of multiple, isolated, and closely spaced, semi-elliptical or thumbnail-shaped cracks located around the weld toe of the brace-to-chord T-joint. It would be most interesting to see the detailed features of the initiation and growth of these thumbnail cracks to gain an understanding of how they interact and coalesce to form longer cracks.

In general, the fracture surfaces were very rough and irregular, typically consisting of deep troughs or valleys and raised or elevated regions. Figure 6(*a*) shows the fracture surface topography typical of the protected areas in the troughs or valleys. It had a fibrous appearance, which may possibly be related to the microstructural features of the underlying steel. The raised or elevated regions sometimes had the appearance of mountain ranges or ridges, and these possibly correspond to grain boundaries. However, more often than not these raised regions had a plateaulike appearance, as indicated by the white circles in Fig. 6(*b*), which suggested that the peaks had been beaten or pounded flat by contacting between the crack faces during the closing portion of the fatigue cycle or the corresponding stage of any opening and closing cycle caused by modal testing. This point will be discussed in more detail later.

Features similar to those observed in specimen 2 were also observed in specimen 3. Clear evidence was found in this specimen that fatigue crack initiation had occurred at welding defects along the weld toe. Figure 7 shows a fatigue crack initiation site in specimen 3. The left-hand side of the figure is the external surface of the T-joint in the region of the weld toe, while the lower right region of the figure is the fatigue fracture surface. The open arrow indicates the direction of local fatigue crack growth. The region marked "P" in this figure is an area of shrinkage porosity in a resolidified region of the once liquid pool of the weld metal. It contains a number of isolated small grains or particles of resolidified weld metal or nonequilibrium second-phase particles.

The plastic deformation and tearing of metal at the tip of a growing fatigue crack often leaves behind a pattern of surface markings in the form of parallel lines or striations on the fracture surfaces. Striations, as shown in Fig. 8, appear on the fracture surface as ripples on a pond, radiating outward from the point of crack initiation and lying approximately perpendicular to the direction of fatigue crack growth. The arrows in Fig. 8 indicate the directions of fatigue crack growth. These fatigue striations were found primarily in the depressed regions of the fracture surface; that is, in the troughs and valleys that were protected from damage caused by the beating or pounding of the fracture surfaces during crack closure.

Evidence of crack closure, such as that shown in Fig. 6(*b*), were found in both specimens. In the case of specimen 3, where indeed the evidence was abundant, the closure damage may have been produced during the closing period of each fatigue cycle. In this case, at a load ratio of zero, the crack faces should be fully closed at the minimum load, and the crack faces should be in intimate contact. Closure-induced damage is expected as a result of fatigue. This is further elucidated in a model for contact of crack surfaces (Sehitoglu and Garcia, 1997). In the case of specimen 2, fatigue tested at $R = 0.2$, the crack faces should never be fully closed during fatigue, and therefore the opportunity for closure damage during fatigue is minimal. Normally, during ΔK-increasing fatigue crack growth at a positive load ratio, the closure force is minimal and the impacting and flattening of crack surfaces is not evident (Wu et al., 1995). These observations strongly suggest that the cracks in the present case have not only experienced fatigue loads, but also additional excitation forces during modal testing that have been sufficient to cause crack closure and fracture surface pounding, which may be considered as inertia-induced crack closure. The inertia forces generated at frequencies near resonance (during modal testing) would add to the nominal compressive load to

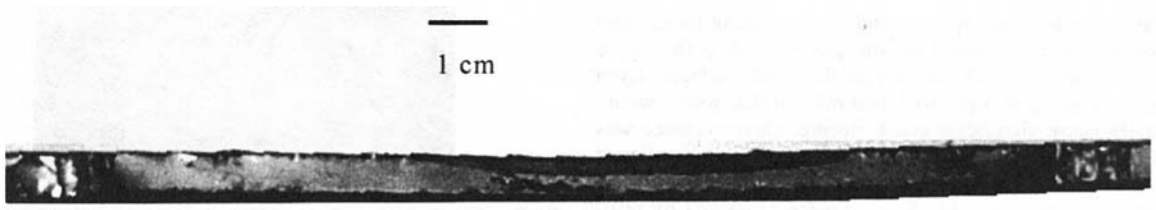

Fig. 5 Photo of crack profile for specimen 3, side 1

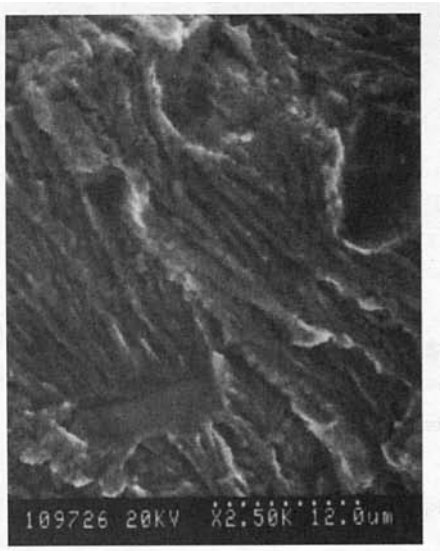

(a)

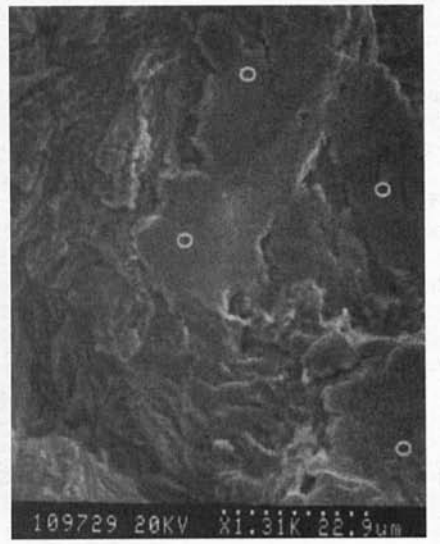

(b)

Fig. 6 Fracture surface features of (*a*) the trough area showing the texture, and (*b*) flattened areas showing the evidence of crack closure in specimen 2, as indicated by the white circles

produce a large closure force that would be sufficient to deform the micro-fracture features of the local high areas of the fracture surface and produce plastically flattened plateaus. This provides evidence of severe beating of the crack surfaces during the modal testing.

In summary of the foregoing fractographic observations, it may be concluded that small fatigue cracks, initially in thumbnail form, were first generated at multiple sites along the weld toe during fatigue. These cracks grew and coalesced to form a large semi-elliptical crack which then continued to grow to become a through-the-thickness crack. Crack opening and closing during fatigue and modal testing were evidenced by the presence of both fatigue striations and the deformed plateaus on the crack surfaces. Even under fatigue loading at a positive load ratio of 0.2, which would not normally cause significant crack closure, clear evidence was found of deformed areas on the crack surface, which are believed to be caused by the repeated pounding (opening and closing) of the two mating surfaces driven by the inertia forces caused by resonance during modal testing.

Fig. 7 A crack initiation site near the surface of the weld toe, for specimen 3. The arrow indicates the direction of crack growth.

The foregoing metallurgical observations and discussion help us to understand the mechanical fatigue behavior of the tubular T-joints as reported in the following sections.

5 Description of Crack Growth

Since most of the fatigue life of specimen 3 appeared to be associated with the growth of a single dominant crack, its data is suitable for a standard fracture analysis. The values of crack length and depth in specimen 3 were plotted against the cycle numbers, as shown in Figs. 9 and 10, respectively. From Fig. 9, and referring to the crack profiles shown in Fig. 5, it appears that crack growth can be divided into two stages: I) the growth of a semi-elliptical crack before it breaks through the thickness, and II) the growth of a through-the-thickness crack. At each stage, fatigue crack growth can be described by a Paris-type equation

$$da/dN = Ba^m \tag{1a}$$

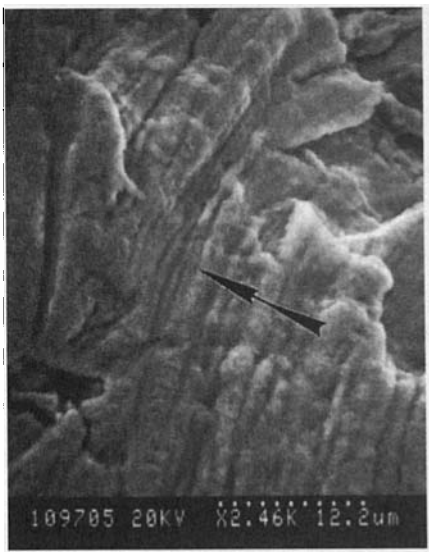

Fig. 8 Fatigue striations in some trough areas, in specimen 3. The arrow indicates the direction of crack growth.

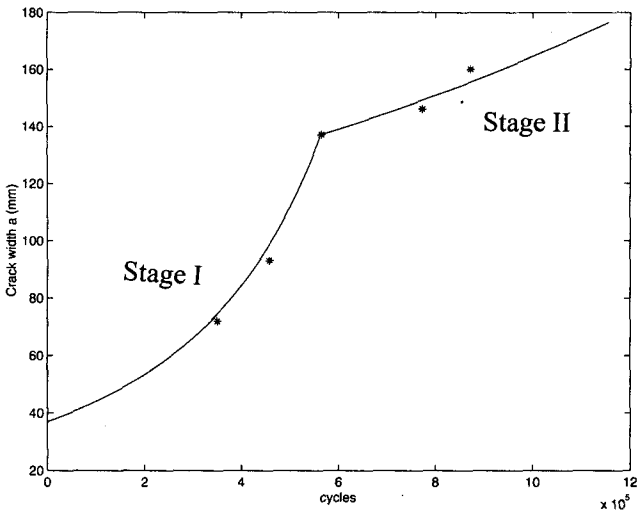

Fig. 9 Experimental observations (*) of crack width as a function of the number of cycles in fatigue for specimen 3. The line represents the interpolation of LEFM.

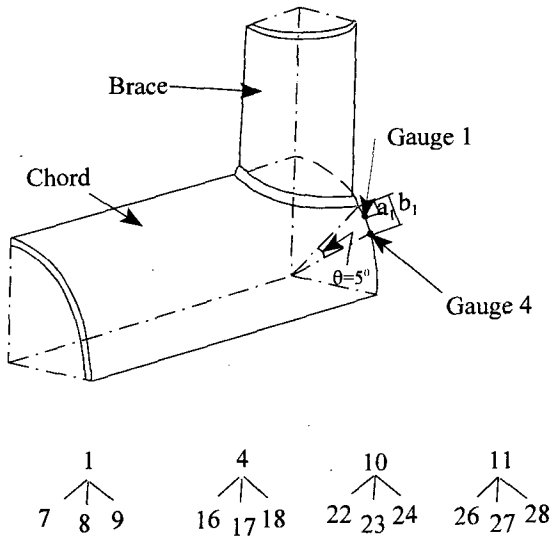

Fig. 11 Gage locations

Integration of Eq. (1*a*) leads to

$$BN = \frac{1}{m-1}\left(\frac{1}{a_0^{m-1}} - \frac{1}{a^{m-1}}\right) \qquad (1b)$$

where a is the current crack length, a_0 is the initial crack length, and N is the number of fatigue cycles. Then, Eq. (1*b*) is used to fit the experimentally observed crack growth data in Fig. 9. The values of the fitting constants B, m, and a_0 are given in Table 3.

It is interesting to note that B and m values for the two stages of crack growth are almost identical, which indicates that fatigue crack growth followed the same law whether it grew as a semi-elliptical crack or a through crack.

In Fig. 9, the back-extrapolation value of Stage I curve at N = 0 only assumes that an initial crack of size 37 mm would have existed had the crack growth process started from a single crack. However, in reality as shown in the fractographic pictures, the fatigue crack was most likely formed by the coalescence of a number of smaller thumbnail cracks at a very early stage. Unfortunately, the early stages of crack nucleation, growth, and coalescence were not recorded in this study; thus, a quantitative interpretation of crack initiation and growth before 3×10^5 cycles is missing. The back-extrapolation value of the Stage II curve assumes the initial crack length had it started to grow as a through-the-thickness crack. These two values are only parameters in the equation, but do not necessarily represent the real-world situation as discussed in the foregoing.

From Fig. 10, it appeared that crack growth in the thickness direction had followed a linear behavior at a constant growth rate of $da/dN = 1.6 \times 10^{-5}$ mm/cycle.

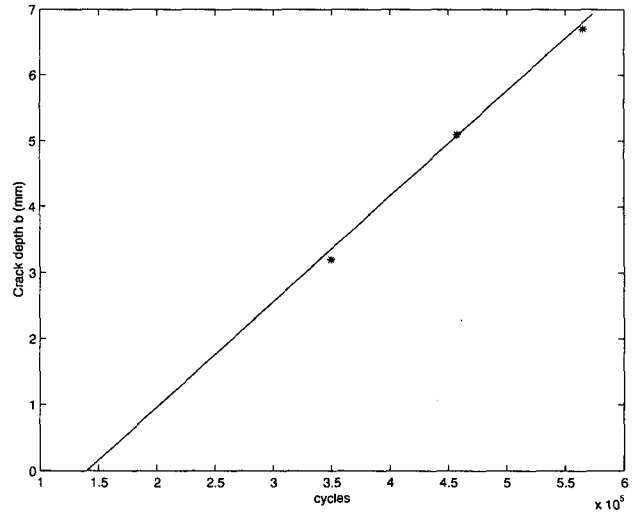

Fig. 10 Experimental observations (*) of crack depth as a function of the number of cycles in fatigue for specimen 3. The line represents the observed behavior. $N = 1.4 \times 10^5 + 6.25 \times 10^4 b$.

Table 3 Fitting constants for crack growth curves

Stage	Cycles (N)	B	m	a_0 (mm)
I	$N < 5.65 \times 10^5$	2.273×10^{-7}	1.55	37
II	$N > 5.65 \times 10^5$	2.273×10^{-7}	1.6	137

6 Static Response During Fatigue Crack Growth

During fatigue testing, static strains were continuously monitored using 120 Ω rosette gages at two locations on each side of the chord. The exact locations of these gages are shown in Fig. 11 for the major cracking side as gage number 1 (channels 7, 8, 9) and 4 (channels 16, 17, 18). In this study, $a_1 = 0.2(rt)^{1/2} = 5.6$ mm, $b_1 = R\pi\theta/180 = 22.1$ mm (with $\theta = 5$ deg in Fig. 11), which are the traditionally recommended locations for fatigue testing of tubular T-joints. The static strains were measured at these locations under the maximum fatigue loads given in Table 2.

Plotting the relative strains ϵ/ϵ_0 (the ratio of the fatigue strain ϵ to the initial static strain ϵ_0) against the logarithm of the number of fatigue cycles N, a general trend of decreasing ϵ/ϵ_0 with log N is observed for all the three specimens, as shown in Figs. 12 and 13 at the two different gage locations 1 and 4, respectively. By this normalization, the static strain data taken at different gage points fall close to a curve (which will be discussed later in detail) for each specimen. The relative strain remained fairly constant for a certain number of fatigue cycles, then it fell steeply as log N increased. The turning point in the ϵ/ϵ_0 versus log N relation was observed to be approximately 10^4 for specimens 1 and 3, where the cracking process appeared to be dominated by the growth of a single crack, first in semi-elliptical form and then as a through-crack as shown in Fig. 5, but the turning point for specimen 2 was about 10^6 cycles. In this specimen, the cracking process consisted of successive nucleation, growth, and coalescence of a number of small thumbnail cracks as shown in Fig. 4. These observations indicate that the changes in static strains are sensitive to the

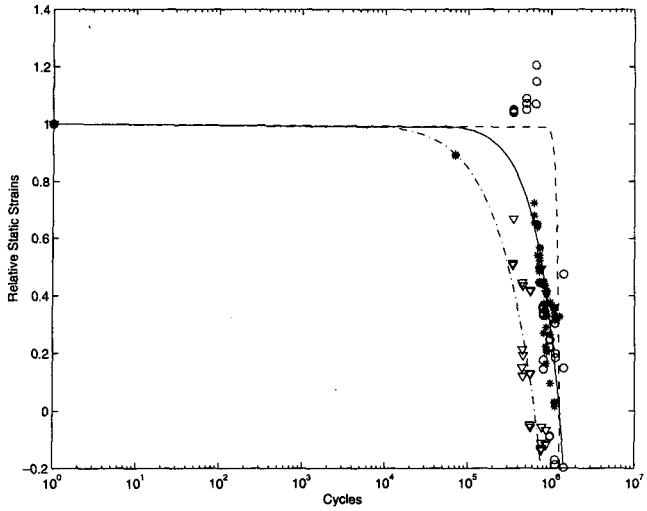

Fig. 12 The observation of static strain (at gage 1) as a function of the number of cycles in fatigue (*: specimen 1; ○: specimen 2, △: specimen 3). The lines are obtained from equation ("--": specimen 1; "- -": specimen 2, "-." specimen 3).

presence of large cracks, formed either by growth of a single crack or by coalescence of a number of thumbnail cracks, but rather insensitive to the initiation of small thumbnail cracks. This scenario was not totally unexpected because the formation of individual thumbnail cracks causes only a minimal loss of load-bearing area. Only when these small cracks had joined to form a large crack did the loss of load bearing area begin to influence the strains at the gauge points. In Fig. 12, one may notice some abnormality such that the relative strain increased above 1.0 before it dropped with further crack growth. This was because at this point the two larger thumbnail cracks were about to join together, but before their coalescence, the ligament connecting the two crack fronts was highly stressed, and therefore the local strains were high. After the coalescence, the load-bearing area was lost and traction-free surfaces were created, and subsequently strain fell abruptly. This process can be envisaged by referring to Fig. 4. Note that the coalescence point was in close alignment with the strain gage. Indeed, although the specimens were nominally identical in geometrical design and were under similar fatigue loads, the fatigue cracking process in each specimen was different due to variations in the defect distribution along the weld toe, as described by the three curves in Figs. 12 and 13.

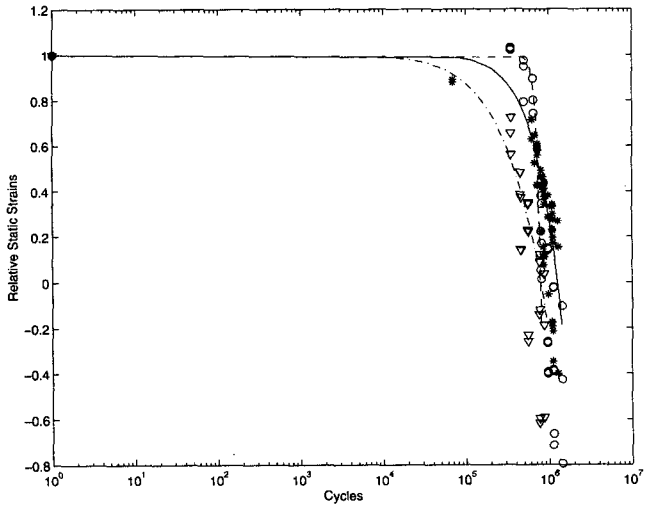

Fig. 13 The observation of static strain (at gage 4) as a function of the number of cycles in fatigue ("*" specimen 1; "○" specimen 2, "△" specimen 3). The lines are obtained from equation (--: specimen 1; - -: specimen 2, -. specimen 3).

Table 4 Equation constants

Gage no.	Specimen	A	n
1	1	6.1	0.05
	2	6.1	0.005
	3	5.8	0.08
4	1	6.1	0.05
	2	5.9	0.008
	3	5.9	0.08

To summarize the general trend of the variation of the static strain with fatigue crack growth in the tubular T-joints, we use a power law equation to describe the logarithmic variation of the number of fatigue cycles with the relative change of static strain during fatigue, as

$$\log_{10} N = A(\Delta\epsilon/\epsilon_0)^n \tag{2}$$

where $\Delta\epsilon = \epsilon - \epsilon_0$ is the change in the static strain caused by cracking; A can be defined as the logarithmic life at 100 percent strain change, i.e.,

$$A = \log_{10} N|_{\Delta\epsilon/\epsilon_0=1} \tag{3}$$

and n is defined as the strain sensitivity index.

With Eq. (2), the relative fatigue life (or health level) of the T-joint can be monitored. Table 4 lists the values of A and n for each specimen. It is interesting to note that, for all the three specimens fatigued under similar loads, the logarithmic life parameter $A(\approx 6)$ is approximately a constant, but n varies between 0.005 to 0.08. This observation suggests that A depends largely on the amplitude of the fatigue load, whereas n is sensitive to the crack profile and configuration. The fitting of Eq. (2), at all $\Delta\epsilon/\epsilon_0$ values, is within a factor of 2. Therefore, Eq. (2) may be suitable for monitoring the fatigue crack growth process in tubular T-joints within a reasonable error band. Using this relationship in structural monitoring, it would allow maintenance engineers to detect fatigue cracks in the structure well before they could cause catastrophic failure.

7 Conclusions

In this study, full-scale tubular T-joint fatigue tests have been conducted. It was found that static strains could be used to monitor crack growth over a significant portion of the life span of the joints. Major observations have been made as follows:

1 Cyclic loading of these tubular T-joints, under the conditions employed in this study, has been shown to give rise to fatigue cracking, which occurs by the formation of small, surface connected thumbnail cracks at the weld toe.

2 The thumbnail cracks initiate at multiple sites, either simultaneously or in close succession, and their growth eventually leads to interlinking and the resulting formation of cracks of high aspect ratio (surface length to depth), and eventually to through-the-thickness cracks. A Paris-type equation can be used to describe fatigue crack growth before and after the breakthrough of the crack through the wall thickness.

3 Strain gages were employed to monitor crack growth since strain gage data reflects the deformation state of the structure. The change in the static strains, associated with the aforementioned crack growth processes, in tubular T-joints has been found to follow a characteristic equation of the following form:

$$\log_{10} N = A(\Delta\epsilon/\epsilon_0)^n$$

This equation may be used for nondestructive detection of cracks before they reach critical dimensions. In combination with the

Paris equation, the foregoing equation can also be used to predict the fatigue life for offshore structures.

4 Fracture surfaces have been analyzed using SEM techniques. In addition to features of crack initiation and propagation, such as ridges originating from porosity sites (Fig. 7) and striations (Fig. 8), evidence of crack closure has been found. This has the appearance of flattened plateaus (Fig. 6(*b*)) on the fracture surfaces, which indicates severe pounding between the two mating surfaces during modal testing at the frequencies near the resonance frequencies. The pounding is believed to be driven by the inertia force. Thus, this type of crack closure may be regarded as inertia-induced crack closure which is a resonant vibration phenomenon.

References

Bouwkamp, J. G., 1966, "Tubular Joints under Slow-Cycle Alternating Loads," *Proceedings, International Symposium on the Effect of Repeated Loading on Materials and Structures,* RILEM, Mexico City, Mexico, Vol. VI.

Cheng, S. M., Swamidas, A. S. J., Wallace, W., and Wu, X. J., 1999, "Nondestructive Detection of Cracks in Tubular T-Joints Using Vibration Characteristics," ASME JOURNAL OF OFFSHORE MECHANICS AND ARCTIC ENGINEERING, Vol. 121, Aug., pp. 144–152.

Dijkstra, O. D., and deBack, J., 1980, "Fatigue Strength of Tubular T and X-Joints," Paper No. 3696, *Proceedings, Offshore Technology Conference,* Houston, TX.

Dover, W. D., and Holdbrook, S. J., 1979, "Fatigue Crack Growth in Tubular Welded Connections," Paper No. 40, *Proceedings, 2nd International Conference on Behavior of Offshore Structures,* London, U.K.

Gibstein, M. B., 1981, "Fatigue Strength of Welded Tubular Joints Tested at Dnv Laborations," Paper No. TS 8.5, *Proceedings, International Conference on Steel in Marine Structures,* Paris, France.

Gurney, T. R., 1989, "The Influence of Thickness on Fatigue of Welded Joints—Ten Years (A Review of British Work)," *Proceedings, VIIIth International Conference on Offshore Mechanics and Arctic Engineering,* the Netherlands, pp. 1–8.

Lambert, S. B., Mohaupt, U. H., Burns, D. J., and Vosikovsky, O., 1987, "Simulation of Fatigue Behavior of Tubular Joints Using a Pipe-to-Plate Specimen," *Proceedings, IIIth International Conference on Steel in Marine Structures,* the Netherland, pp. 489–500.

Leiurade, H. D., and Gerald, J., 1981, "Experimental Results of Fatigue Tests on Ten Full Scale X Joints," Paper TS 6.4, *Proceedings, International Conference on Steel in Marine Structures,* Paris, France.

Linda, K., et al., 1981, "A Fatigue Design Procedure for Offshore Tubular Connection," Paper No. 11, *Proceedings, 2nd International Conference on Integrity of Offshore Structures,* ed., D. Faulkver, Glasgow, Scotland, U.K.

Maeda, T., et al., 1969, "Experimental Study on the Fatigue Strength of Welded Tubular T- and X-Joints," IIW Doc. No. XV-270-69.

Natarajan, M., and Toprac, A. A., 1968, "Research on Fatigue Strength of Tubular T-Joints," Report of Structural Fatigue Research Laboratory, University of Texas, Austin, TX.

Pedersen, N. T., and Agerskov, H., 1991, "Fatigue Damage Accumulation in Offshore Tubular Structure under Stochastic Loading," *Tubular Structures, 4th International Symposium,* pp. 269–280.

Recho, 1990, "Probabilistic Approach to Fatigue Life in T-Welded Tubular Joints," *Tubular Structures, 4th International Symposium,* pp. 254–265.

Sehitoglu, H., and Garcia, A. M., 1997, "Contact of Crack Surfaces during Fatigue: Part 2. Simulations," *Metallurgical and Materials Transactions A,* Vol. 28A, pp. 2277–2289.

Wu, X. J., Wallace, W., and Koul, A. K., 1995, "A New Approach to Fatigue Threshold," *Fatigue and Fracture of Engineering Materials and Structures,* Vol. 18, pp. 833–845.

Wylde, J. G., 1983, "Fatigue Tests on Welded Tubular T-Joints with Equal Brace and Chord Dimensions," Paper No. DTC 4527, *Proceedings, Offshore Technology Conference,* Houston, TX.